Multiscale entanglement in ring polymers under spherical confinement

Luca Tubiana[1], Enzo Orlandini[2], Cristian Micheletti[1]

[1] SISSA - Via Bonomea 265 - I-34136, Trieste - Italy

[2] Dipartimento di Fisica "G. Galilei" and Sezione INFN - Via Marzolo 8 - I-35100 Padova, Italy

The interplay of geometrical and topological entanglement in semiflexible knotted polymer rings confined inside a spherical cavity is investigated using advanced numerical methods. By using stringent and robust algorithms for locating knots, we characterize how the knot length l_k depends on the ring contour length, L_c and the radius of the confining sphere, R_c. In the no- and strong-confinement cases we observe weak knot localization and complete knot delocalization, respectively. We show that the complex interplay of l_k, L_c and R_c that seamlessly bridges these two limits can be encompassed by a simple scaling argument based on deflection theory. The same argument is used to rationalize the multiscale character of the entanglement that emerges with increasing confinement.

If we tie a knot in a piece of rope and pull the latter at its extremities, the knotted part will become readily distinguishable from the rest of the rope because it localizes. Indeed, for a very long rope only a neglible fraction of its contour length will be required to accommodate the knot [1]. In this intuitive example of *knot localization* the topological (global) entanglement embodied by the knot does not interfere with the geometrical (local) entanglement of the rest of the rope. This is hardly the case for polymers that circularize in equilibrium. In such rings, knots are abundant [2] and the interplay between topological and geometrical entanglement impacts significantly the molecules' dynamical, mechanical and metric properties [3–5]. Understanding how and to what extent global and local entanglement are related is a major open issue in polymer physics [6] with ramifications in key biological contexts[7], especially those related to genome organization in eukaryotes, bacteria and viruses [8–12].

A first breakthrough in the problem could be made by establishing what fraction of the polymer ring is occupied by the knot(s) and whether this measure is sufficiently robust or depends instead on the geometrical entanglement degree. As a prototypical context to examine this problem we consider semi-flexible, self-avoiding rings of cylinders with the simplest knotted topology, a 3_1 (trefoil) knot, and subject to isotropic spatial confinement. In such a system, by varying the size of the confining region, the degree of geometrical complexity can be changed and related to the equilibrium size of the knotted ring portion.

For definiteness, the rings properties are set to match dsDNA. Specifically, the cylinder diameter and long axis are set equal to $d = 2.5nm$ and $b = 10nm$, respectively. The latter quantity is ten times smaller than the DNA Kuhn length (equal to twice the persistence length, $l_p = 50nm$) thus ensuring a fine discretization of the model DNA. The system energy includes steric hindrance of non consecutive cylinders plus a bending potential:

$$E_b = -K_b T \frac{l_p}{b} \sum_{i=1}^{N} \vec{t}_i \cdot \vec{t}_{i+1} \tag{1}$$

where $\vec{t}_i$ is the orientation of the axis of the ith cylinder, $\vec{t}_{N+1} \equiv \vec{t}_1$ and the temperature T is set to 300K. We considered rings of $N = 50, ...250$ cylinders, corresponding to countour lengths, $L_c = Nb$ ranging from $500nm$ to 2.5 μm. This range allows for probing changes in knot localization going from semiflexible to fully-flexible rings [13] as well as examing the effect of the interplay between L_c, l_p and the radius of the confining sphere, R_c. For simplicity of notation in the following all lengthscales are expressed in units of b.

Because compact ring configurations are entropically disfavoured with respect to unconstrained ones, simple stochastic sampling schemes cannot be effectively used to generate spatially confined rings [6]. An analogous entropic attrition works against having a sizeable population of knots of a given type, trefoils in our case, at all levels of confinement [6]. To overcome these two difficulties we used a biased Multiple-Markov-chain sampling scheme [12] with 24 Markovian replicas. For each replica, ring configurations are evolved using crankshaft and hedgehog Monte Carlo moves [14]. The moves preserve the length of the rings, but not the topology, consistently with ergodicity requirements [6, 15]. In fact, even when the configurations before and after the move are self-avoiding, the move itself may involve self-crossings of the chain. A newly generated ring, Γ, is accepted according to the standard Metropolis criterion with canonical weight, $\exp\left[-U(\Gamma)/K_B T\right]$, where the potential energy, U is suitably chosen to enhance the populations of compacts trefoil rings. Specifically, if Γ is non self-avoiding or has a too complicated topology (8 or more minimal crossings according to the Alexander polynomial [6]) then U is set equal to infinity, otherwise $U(\Gamma) = E_b(\Gamma) + p\,R_c(\Gamma)$. In the latter expression, R_c is the radius of the sphere containing Γ (calculated as the largest distance of the cylinder vertices from the ring geometric center) and p is a confining field whose value is set differently for the various replicas so to sample rings with different degree of confinement.
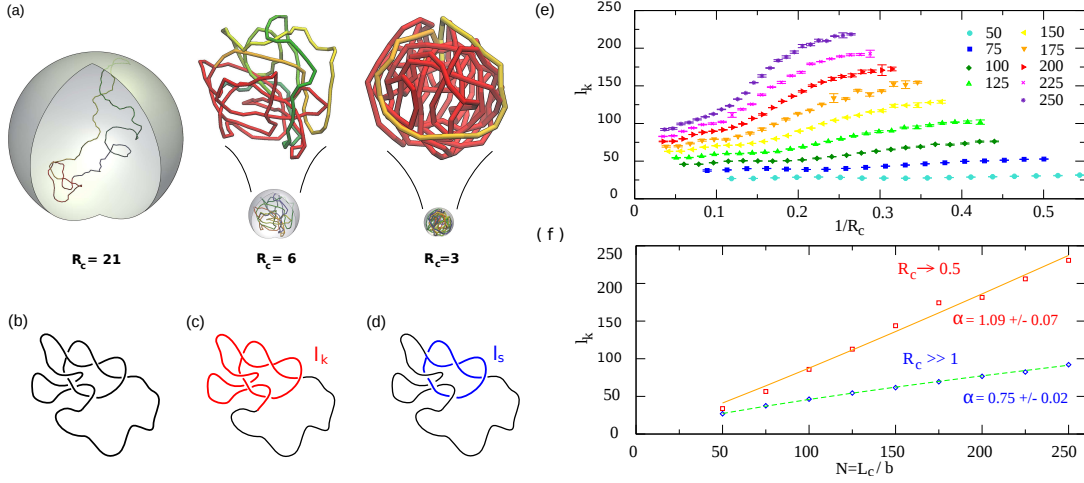
FIG. 1. (a) Typical configurations of trefoil-knotted rings with $N = 200$ cylinders at different levels of confinement. The encapsidated configurations for $R_c = 6$ and $R_c = 3$ are magnified for ease of visualization. The knotted portion of the rings is shown in red. (b) Sketch of a trefoil-knotted ring; its knotted portion is highlighted in red in panel (c) and its shortest knotted arc is shown in blue in panel (d). (e) Average knot length, l_k, as a function of $1/R_c$ for rings of varying number of cylinders, $N = 50...250$. (f) Dependence of l_k on L_c in the no- and strong-confinement limits; the lines represent the best-fitting power laws. The strong-confinement data correspond to the limiting values approached exponentially by the curves in panel (e). The exponential fit was limited to the data points for which $l_k > 0.6L_c$.

For each value of N this procedure was used to generate at least $\sim 10^7$ configurations with varying compactness and topology. For the *a posteriori* data analysis we picked, out of the generated rings, an uncorrelated subset with 3_1 topology (positively established with the KNOTFIND algorithm [16]). Finally a thermodynamic reweighting technique [12] is used to remove the p bias and obtain canonical averages for the observables.

Figure 1a illustrates both the range of spherical confinement spanned by the sampled rings as well as the arclength covered by the knot. As a first method to identify the knotted portion we look for the arc, Γ_1, that (i) has the 3_1 topology while the complementary subchain, $\Gamma_2 \equiv \Gamma \setminus \Gamma_1$ is unknotted; (ii) cannot be further shortened without losing the full-ring 3_1 topology and finally (iii) can be extended continuously to encompass the whole ring retaining the 3_1 topology and the unknottedness of the complementary arc, Γ_2. The topological state of the open arcs Γ_1 and Γ_2 is established after bridging their termini with the minimally-interfering closure of ref. [17].

The above scheme for locating the knot can be seamlessly and robustly applied at all levels of ring compactification. As such, it considerably extends the scope of previous investigations where, depending on the free or collapsed nature of the rings, the knotted-arc identification had to be made with different and inequivalent methods, including ones affecting chain geometry by a rectification procedure or by external constraints such as a sliplink[18, 19].

Two important facts emerge from Fig. 1e: for a given ring contour length, L_c, the increased confinement is parallelled by an increase of the length of the knotted arc, l_k; at the same time, for a given size of the confining sphere one has that l_k increases with L_c. As a first step towards a comprehensive rationalization of the results we examine the l_k versus L_c behaviour in the no- and strong-confinement limits, which are shown in Fig. 1f.

In the unconstrained case, it is seen that l_k increases as a power of L_c: $l_k(R_c \to \infty) \propto L_c^\alpha$ with $\alpha = 0.75 \pm 0.02$. The sublinear increase implies that l_k/L_c vanishes for increasing L_c, resulting in a weak knot localization. This is consistent with previous results on knot localization for unconstrained rings both on- and off-lattice where, however, different values of α ranging from 0.54 to 0.75 were reported [18, 19]. It also agrees qualitatively with recent experimental findings on knotted circular DNA adsorbed on mica surfaces based on single molecule imaging techniques [20].

A power-law dependence of l_k on L_c provides a good fit of the data for strong confinement too but in this case $\alpha = 1.09 \pm 0.07$. This is compatible with a linear dependence of l_k on L_c thus implying a full delocalization of the knot in equilibrated rings subject to severe three-dimensional confinement. To the best of our knowledge this fact has not been established before. However, it is worth pointing out that knot delocalization has been previously observed for θ-collapsed knotted rings [18, 19]. The analogy with our findings is noteworthy since the ring metric properties are dictated purely by equilibrium thermodynamics for collapsed rings while spatial constraints are also at play for confinement.

We next turn our attention to the intermediate regime intervening between the no- and strong-confinement limits and show that the complex behaviour of Fig. 1e can be rationalized in terms of a surprisingly simple relationships involving the length scales L_c, R_c and l_k.
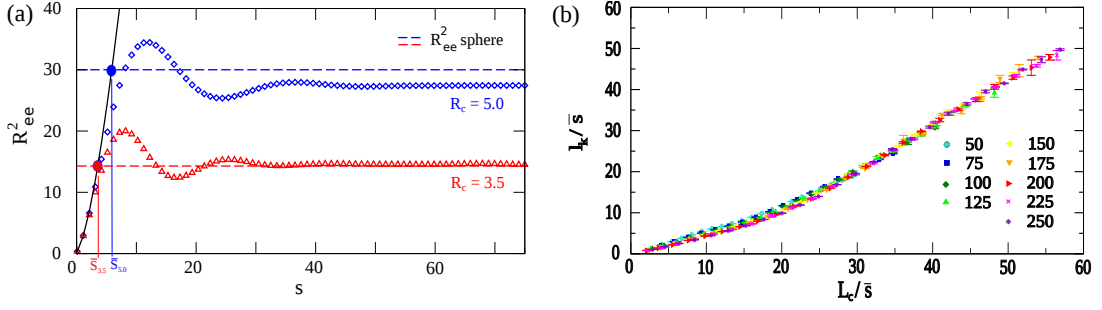
FIG. 2. (a) Mean squared end-to-end distance, R_{ee}^2, of arcs of length s in rings of $N = 150$ cylinders at different levels of confinement. The dashed horizontal line indicates the reference value equal to $6/5R_c^2$ while the continuous line shows the expected R_{ee}^2 for an unconstrained, non-self-avoiding Kratky-Porod (KP) chain. The intersection of these reference lines determines the nominal deflection arclength, $\bar{s}$ highlighted by the dropline. (b) Collapse of the same data points as in Fig. 1e obtained by rescaling l_k and L_c by $\bar{s}$. The slope of the line fitting the data for $\frac{L_c}{\bar{s}} > 40$ is 1.09 ± 0.02.

To this purpose we first observe that upon increasing confinement the geometric characteristics of the rings resemble those of uniformly filled spheres. In particular the eigenvalues of the tensor of gyration of rings become close to the eigenvalue of a uniformly-filled sphere (see supporting material).

The approximately uniform filling of the confining sphere by mildly- or strongly-confined rings is well illustrated in Fig. 2a which portrays the mean squared end-to-end separation, $R_{ee}^2(s)$ of ring portions of different arclengths, s. In fact, the profile of $R_{ee}^2(s)$ is noticeably flattened and its plateau value is about $6/5R_c^2$, which is the mean square distance of two points inside a spherical volume of radius R_c. The value of s at which the plateau value of R_{ee}^2 is reached corresponds to the typical contour length, $\bar{s}$, of a discrete worm-like (Kratky-Porod) chain with mean squared end-to-end distance equal to $6/5R_c^2$

$$R_{ee}^2(\bar{s}) = 2l_p\bar{s}\left[1 - \frac{l_p}{\bar{s}}\left(1 - e^{-\frac{\bar{s}}{l_p}}\right)\right] = \frac{6}{5}R_c^2 \ . \tag{2}$$

$\bar{s}$ is the nominal arclength of unrestricted ring-portions that are just long enough to hit the sphere boundary and, by inverting (2), can be expressed in terms of the principal branch of the Lambert W function [21],

$$\bar{s}/l_p = 1 + y + W(-\exp[-1 - y]) \tag{3}$$

where $y \equiv 3R_c^2/5l_p^2$. We shall refer to $\bar{s}$ as the deflection arclength, in analogy with the deflection argument originally introduced for polymers in channels [22] and later applied to other contexts, such as crumpled globules [8].

The deflection arclength is crucial for rationalizing the results of Fig. 1e and 1f. In particular it is plausible that confined rings that experience the same nominal number of deflections at the spherical hull boundary should have statistically similar knot lengths once rescaled by $\bar{s}$. This conjecture is supported by the scatter plot of Fig. 2b where the rescaled knot length is plotted against the number of nominal deflections $L_c/\bar{s}$ for rings of all considered lengths, $50 \le N \le 250$, and degrees of confinement. Despite the heterogeneity of the original data sets (see Fig. 1e), the plot displays a striking collapse of the data points. A broadening of the curves is seen only in the limit of unconstrained rings, where indeed, the deflection length looses meaning. We stress that, because $\bar{s}$ is calculated deterministically, no single adjustable parameter was introduced to obtain the collapse in Fig. 2b. The collapsed curve exhibits an asymptotic linear trend thus reinforcing the delocalization result of Fig. 1f.

We conclude the study of the interplay of ring geometry and topology by showing that, by increasing the ring compactification, a non-trivial type and degree of entanglement is observed at progressively smaller arclengths.

To do so we search for the smallest arcs with 3_1 topology. As illustrated in Fig. 1c,d such minimally-long knotted portion may differ from the proper knotted arc introduced before because it does not necessarily satisfy criterion (iii). Consequently, it may correspond to an ephemeral knot (because it can be contained in a longer arc with different topology, e.g. an unknot) [23].

Fig. 3a illustrates how the length of the shortest knotted arc, l_s, behaves for increasing confinement and compares it with l_k. It is seen that for no- or midly-constrained rings, when the ring geometrical entanglement is minimal, the two measures are in good accord. However, upon increasing confinement they progressively diverge. Notice that l_s and l_k provide lower and upper limits to the range of arclengths over which non-trivial topological entanglements (after arc closure) are observed. Consequently, the divergence of the two metrics indicates that the entanglement cannot be described by a single length scale but it displays a multiscale behaviour that amplifies upon increasing confinement. Similarly to the case of the proper knot length, l_k, the concept of deflection arclength is useful for rationalizing the
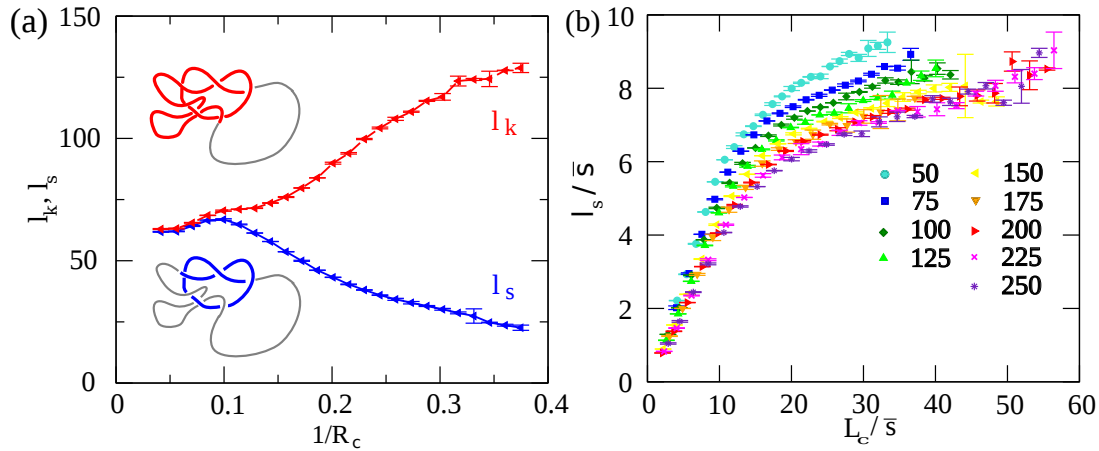
FIG. 3. (a) Dependence of knot length, l_k, and the shortest knot length, l_s, on confinement for rings of $N = 150$ cylinders. (b) Scatter plot of $l_s/\bar{s}$ versus $L_c/\bar{s}$ for rings of all lengths and degree of confinement.

interplay of l_s, R_c and L_c. In fact, l_s expectedly results from the balance between (a) the increasing probability that a knot can be tied with a minimal (nominal) number of deflected segments/cylinders for longer and more confined rings and (b) the decreasing probability that the complementary arc is unknotted.

In the plot of Fig. 3b it is seen that, for increasing L_c, the $l_s/\bar{s}$ data tend to approach a limiting curve that has a linear dependence on $L_c/\bar{s}$. The results indicate that for medium and strong confinement the length of the smallest, and possibly ephemeral, knot l_s increases approximately linearly both with the L_c at fixed R_c and with R_c at fixed L_c (more data in supp. mat.). Together with the behaviour of l_k, the results provide a quantitative basis for the multiscale character of the ring entanglement that sets in for increasing confinement.

To summarize, we have used simulations to measure the length of the topologically entangled portion (l_k) of knotted self-avoiding ring polymers subjected to different degree of spherical confinement. We find that for weak confinement, when the geometrical entanglement of the chain is moderate, the knot is weakly localized while for strongly packed rings it delocalizes completely. The delocalization trend at increasing confinement and different L_c follows the neat scaling behavior of Fig. 1f which is rationalised in terms of the deflection arclength. The latter therefore appears to be a key quantity to characterize the complex interplay of the geometry and topology in confined polymer rings, which reverberates in the above mentioned multiscale entanglement. This observation prompts the question of whether an analogous concept and scaling argument can be introduced to characterize and rationalize the entanglement found in other systems of densely-packed circular polymers, such as ring melts or theta-collapsed rings [8, 18, 19]. We wish to point out that our results have direct bearings on the relevant problem of viral DNA ejection into infected cells [24]. In fact this crucial step of the viral infection is not hindered by the presence, in the packaged genome, of knots because the latter are highly delocalised [7, 11].

[1] G Buck, Nature **392**, 238 (1998); V Katritch *et al*, Phys. Rev. E **61**, 5545 (2000); K Millett, A Dobay, A Stasiak, Macromol. **38**, 601 (2005).
[2] DW Sumners and SG Whittington, J. Phys. A: Math. Gen. **21**, 1689 (1988).
[3] V Katritch *et al*, Nature **384**, 142 (1996).
[4] Y Arai *et al*, Nature **399**, 446 (1999).
[5] SR Quake, Phys. Rev. Lett. **73**, 3317 (1994); NT Moore, RC Lua, AY Grosberg, Proc. Natl. Acad. Sci. USA **101**, 13431 (2004).
[6] E Orlandini, SG Whittington, Rev. Mod. Phys. **79**, 611 (2007); C Micheletti, D Marenduzzo and E Orlandini, Phys. Rep., **504** 1(2011); MD Frank-Kamenetskii, A Vologodskii, Usp. Fiz. Nauk. **134**, 641 (1981).
[7] D Marenduzzo and C Micheletti and E Orlandini, Journal of Physics: Condensed Matter **22**, 283102 (2010).
[8] AY Grosberg *et al*, Europhys. Lett. **23**, 373 (1993); E Lieberman-Aiden *et al*, Science **326**, 289 (2009); A Rosa, R Everaers, PLOS Comp. Biol. **4**, e1000153 (2008); AY Grosberg, Biomat 2010: Int. Symp. on Math. and Comp. Biol., R.P.Mondaini (Editor), World Scientific, Singapore(2011).
[9] S Jun, B Mulder, Proc. Natl. Acad. Sci. USA **103**, 12388 (2006).

[10] J Arsuaga *et al*, Proc. Natl. Acad. Sci. USA **102**, 9165 (2005).
[11] D Marenduzzo *et al*, Proc Natl Acad Sci USA **106**, 22269 (2009).
[12] C Micheletti *et al*, J. Chem. Phys. **124**, 064903 (2006).
[13] K Alim and E Frey, Phys. Rev. Lett. **99**, 198102 (2007).
[14] KV Klenin *et al*, J Biomol Struct Dyn **5**, 1173 (1988).
[15] S Alvarado, J Calvo and KC Millett, J Stat Phys **143**, 102 (2011).
[16] J Hoste and M Thistlethwaite `http://www.math.utk.edu/~morwen/knotscape.html`.
[17] L Tubiana and E Orlandini and C Micheletti, Prog. Theor. Phys. **accepted for publication** (2011), arXiv/1103.0475.
[18] B Marcone *et al*, Phys. Rev. E **75**, 041105 (2007).
[19] P Virnau, Y Kantor, M Kardar, J. Am. Chem. Soc. **127**, 15102 (2005); ML Mansfield, JF Douglas, J. Chem. Phys. **133**, 044903 (2010).
[20] E Ercolini *et al*, Phys. Rev. Lett. **98**, 058102 (2007).
[21] R Corless *et al*, Adv. in Comp. Math. **5**, 329 (1996).
[22] T Odijk, Macromol. **16**, 1340 (1983).
[23] KC Millett, J. Knot Theory Ramif. **19**, 601 (2010).
[24] R Matthews, AA Louis, JM Yeomans, Phys. Rev. Lett. **102**, 088101 (2009).

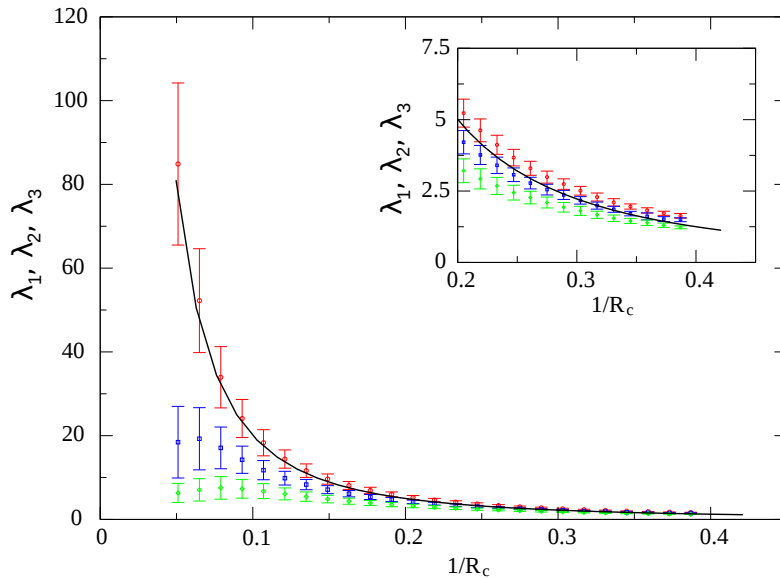# SUPPORTING MATERIAL

A. Size and shape of confined rings

FIG. 4. The average eigenvalues of the rings gyration matrix, λ_1, λ_2, λ_3 (largest to smallest) are shown as a function of the radius of the confining spherical cavity, R_c. Errorbars report the standard deviation around the average value. The inset shows the data for high spatial confinement. Going from no- to mild confinement, the average length of the rings principal gyration axis is substantially reduced while the other two are much less affected. For example, the initial five-fold reduction of λ_1 in rings of $N = 150$ cylinders is accompanied by a change of λ_2 of about 50% and a change of λ_3 not larger than 10%. The latter variation is non-monotonic, indicating a swelling of the mildly confined semi-flexible rings in the plane perpendicular to the (squeezed) primary gyration axis. Importantly, the strong shape anisotropy of unconstrained rings is largely lost even for mild confinement: already at $R_c = 5$ all average gyration are compatible with the gyration eigenvalue of the *uniformly-filled* confining hull within the estimated errors.

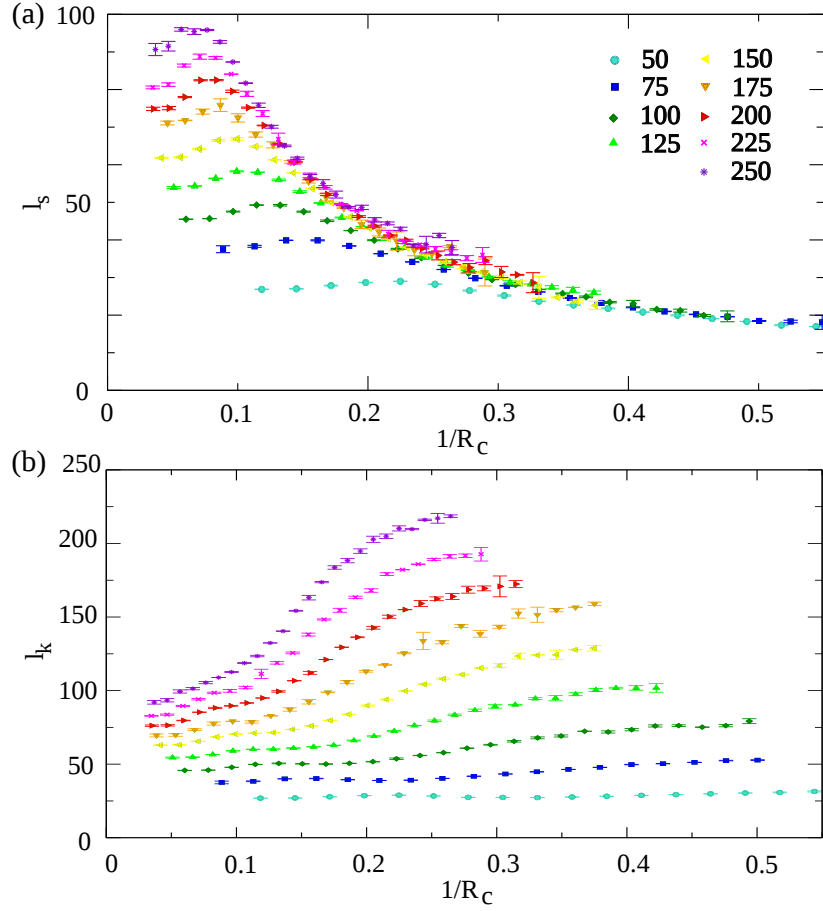## B. Multiscale entanglement: detailed comparison of l_k and l_s

FIG. 5. Average length of shortest knotted arc (a) for rings of different contour lengths L_c and increasing degree of confinement $1/R_c$. Notice that, at a given contour length, l_s becomes smaller for increasing confinement. Also, l_s increases with L_c at fixed degree of confinement. The average length of knotted portion, l_k, shown in Fig. 1 of the manuscript, is reported in panel (b) for ease of comparison.
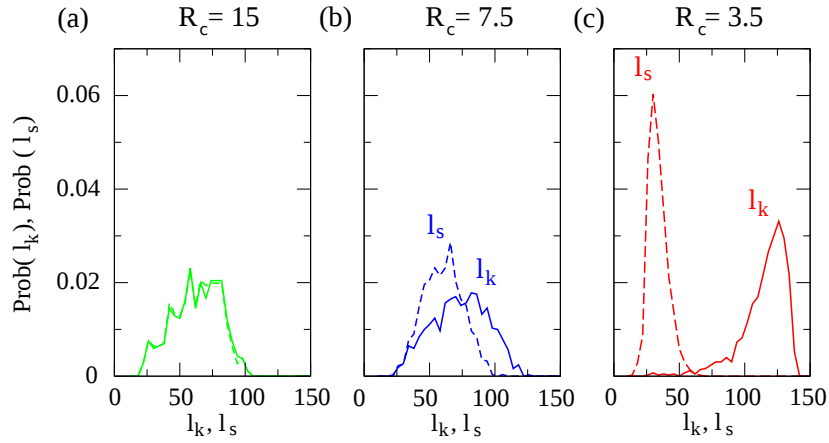

FIG. 6. Probability distribution of the lengths of the shortest knotted arc, l_s, and knotted portion, l_k, at different levels of confinement for rings of $N = 150$ cylinders. At no confinement the two distribution are pratically identical, see panel (a). However, their difference increases progressively with confinement, see panels (b) and (c).

C. Comparison with infinitely thin rings

The robustness and generality of the multiscale character of the entanglement found for self-avoiding rings is underscored by the fact that an analogous phenomenology is found for confined infinitely-thin trefoil-knotted rings, as reported in the following. The infinitely-thin rings are Kratky-Porod chains: they have the same persistence lengths as the self-avoiding ones discussed in the main paper, but have no excluded volume.

Given the absence of steric hindrance, higher levels of compactifications are achieved compared to self-avoiding rings.
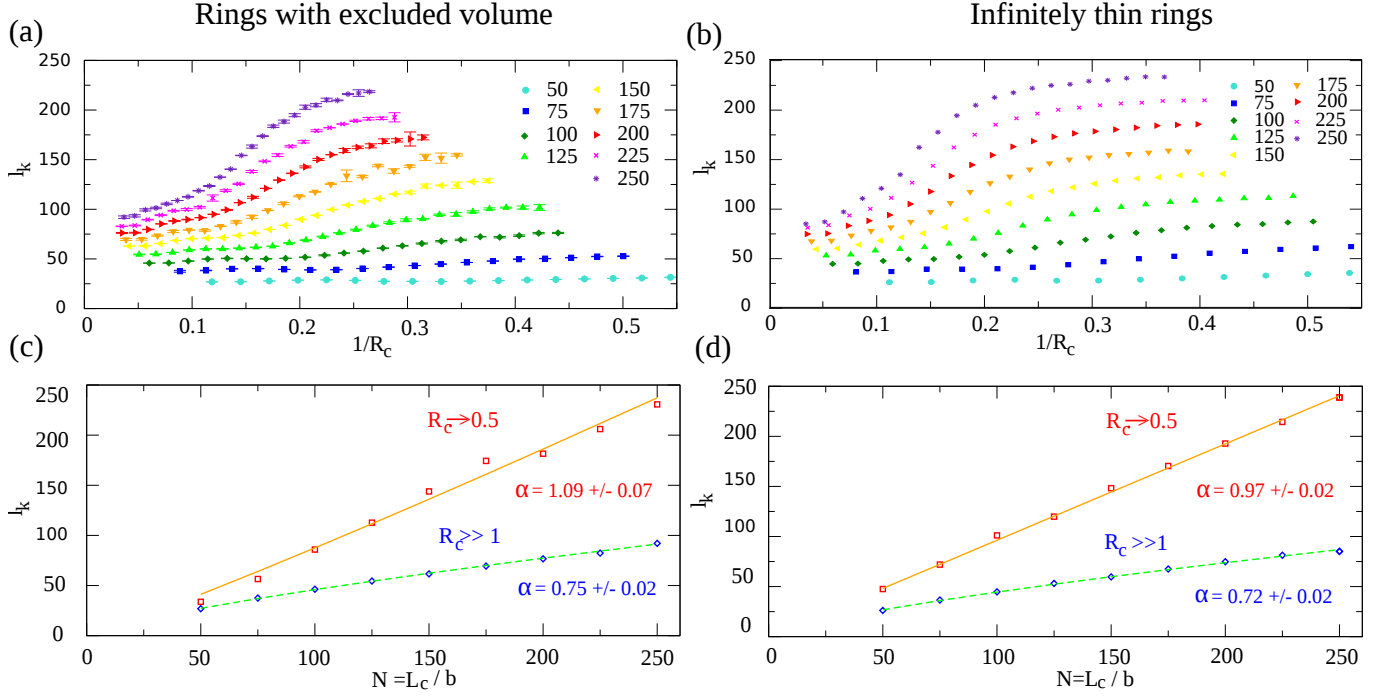

FIG. 7. (a) and (b): average knot length, l_k, as a function of $1/R_c$ for rings with and without excluded volume respectively. (c) and (d): Dependence of l_k with L_c in the no- and strong- confinement limits for rings with and without excluded volume respectively. Note that analogous qualitative behaviour of the two types of models.
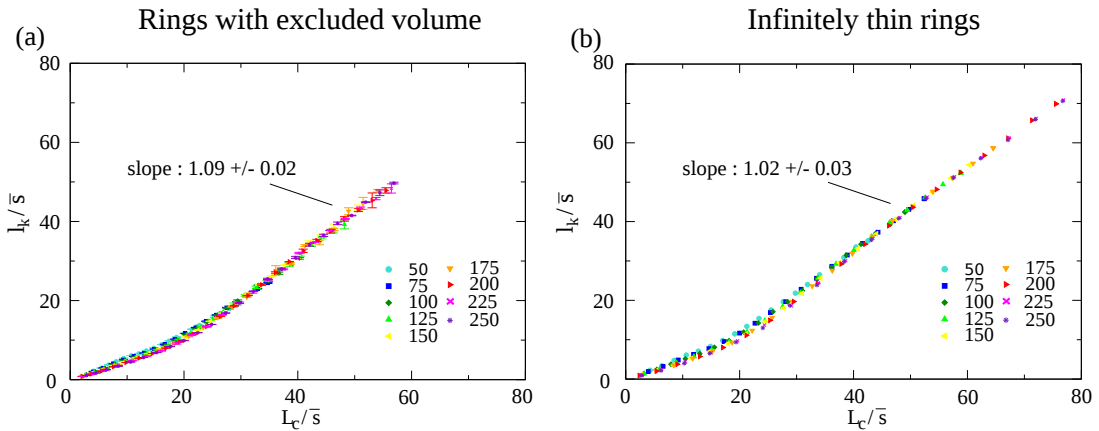

FIG. 8. Collapse of the data points shown in figure 7b (rings with excluded volume, as in main paper) and 7d (rings without excluded volume) obtained by rescaling l_k and L_c by the deflection length, $\bar{s}$. The same deflection length as in eqn. 3 of the main paper was used in both cases. Note that the slope of the line fitting the data for $L_c/\bar{s} > 40$ is compatible between the two cases.
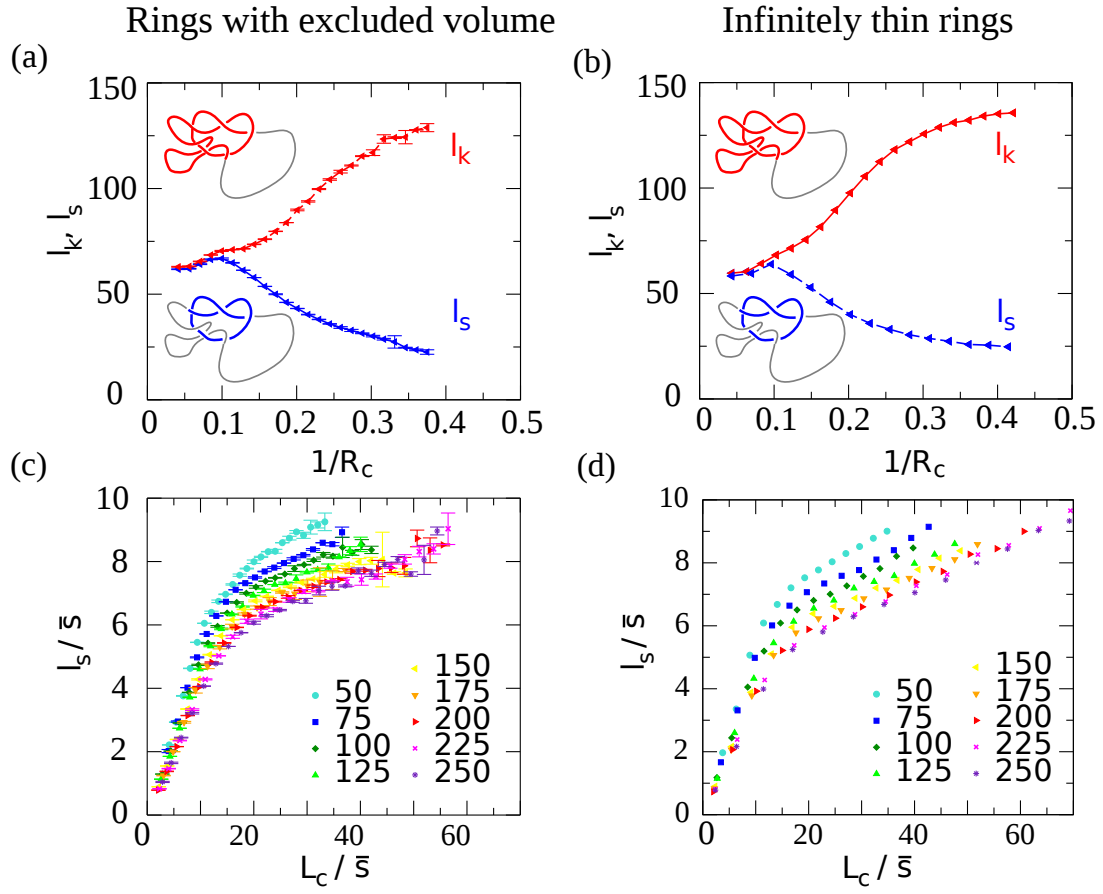
FIG. 9. Top: dependence of knot length, l_k, and the shortest knot length, l_s, on confinement for rings of $N = 150$ segments with excluded volume (panel a) and without excluded volume, (panel b). Bottom: scatter plots of $l_s/\bar{s}$ versus $L_c/\bar{s}$ for rings with excluded volume (panel c) and without excluded volume (panel d).